MNRAS **000**, 1–8 (2016) Preprint 11 January 2017 Compiled using MNRAS LATEX style file v3.0

Dwarf spheroidal J-factors without priors: A likelihood-based analysis for indirect dark matter searches

A. Chiappo[1,2],⋆ J.Cohen-Tanugi[3], J. Conrad[1,2],† L. E. Strigari[4], B. Anderson[1,2], M.A. Sánchez-Conde[1,2]

[1] *The Oskar Klein Centre for Cosmoparticle Physics, AlbaNova, SE-106 91 Stockholm, Sweden*
[2] *Department of Physics, Stockholm University, AlbaNova, SE-106 91 Stockholm, Sweden*
[3] *Laboratoire Univers et Particules de Montpellier, IN2P3/CNRS et Université de Montpellier, 34095 Cedex 05 Montpellier, France*
[5] *Mitchell Institute for Fundamental Physics and Astronomy, Department of Physics and Astronomy, Texas A&M University, College Station, TX 77845, USA*

arXiv:1608.07111v3 [astro-ph.CO] 10 Jan 2017

Accepted 2016 November 24. Received 2016 November 11; in original form 2016 August 25

ABSTRACT

Line-of-sight integrals of the squared density, commonly called the *J-factor*, are essential for inferring dark matter (DM) annihilation signals. The J-factors of DM-dominated dwarf spheroidal satellite galaxies (dSphs) have typically been derived using Bayesian techniques, which for small data samples implies that a choice of priors constitutes a non-negligible systematic uncertainty. Here we report the development of a new fully frequentist approach to construct the profile likelihood of the J-factor. Using stellar kinematic data from several classical and ultra-faint dSphs, we derive the maximum likelihood value for the J-factor and its confidence intervals. We validate this method, in particular its bias and coverage, using simulated data from the *Gaia Challenge*. We find that the method possesses good statistical properties. The J-factors and their uncertainties are generally in good agreement with the Bayesian-derived values, with the largest deviations restricted to the systems with the smallest kinematic data sets. We discuss improvements, extensions, and future applications of this technique.

Key words: galaxies: dwarf – galaxies: kinematics and dynamics – dark matter

1 INTRODUCTION

There exists now a wide range of particle physics models extending beyond the Standard Model of particle physics which accommodate dark matter (DM) candidates. One of the most studied ones features a weakly interactive massive particle (WIMP) (for recent reviews see Bertone et al. 2005, Feng 2010, Conrad 2014), which is expected to yield gamma rays through decay or pair annihilation. The differential photon flux expected from DM annihilation is given by

$$\frac{\mathrm{d}N_\gamma}{\mathrm{d}E_\gamma} = \frac{1}{4\pi} \underbrace{\frac{\langle\sigma v\rangle}{2m_{\mathrm{DM}}^2} \sum_i B_i \frac{\mathrm{d}N_i(E)}{\mathrm{d}E}}_{\text{particle physics factor}} \times \mathrm{J} \quad . \tag{1}$$

Equation (1) describes the dependence of the photon flux on the properties of the candidate particle, such as its mass, m_{DM}, its velocity-averaged thermal cross-section, $\langle\sigma v\rangle$, and the sum of photons in each possible final state i, which has branching ratio B_i and photon yield $\mathrm{d}N_i(E)/\mathrm{d}E$. The last term, the *J-factor*, is the line-of-sight (l.o.s.) integral of the DM halo density ρ_{DM} squared (in the case of annihilation), integrated over a solid angle $\Delta\Omega = 2\pi(1-\cos\theta_{\mathrm{max}})$. It is given by

$$\mathrm{J}(D,\Delta\Omega) = \int_{\Delta\Omega}\int_{\mathrm{l.o.s.}} \rho^2_{\mathrm{DM}}(r(s))\mathrm{d}s\mathrm{d}\Delta\Omega'. \tag{2}$$

Because of this square density dependence of the flux, regions of density enhancements are targets for DM searches. For instance, J $\approx 10^{22}$-10^{23} GeV^2 cm^{-5} for the Galactic centre (GC), 10^{17}-10^{19} GeV^2 cm^{-5} for dwarf galaxies, and 10^{15}-10^{19} GeV^2 cm^{-5} for galaxy clusters (see Conrad et al. 2015 and Charles et al. 2016 for a discussion of different targets for DM searches). These values would place the GC at the top of the candidate targets, however the presence of strong, yet unmodelled fore- and background contaminations renders it a very challenging target (see, for example, Zhou et al. 2015, Calore et al. 2015, Ajello et al. 2016). For this reason and due to the nearly negligible presence of such

⋆ E-mail: andrea.chiappo@fysik.su.se
† Wallenberg Academy Fellow

© 2016 The Authors

contaminations, dSphs are considered the ideal targets for gamma-ray DM searches.

Assuming that DM uniquely consists of WIMPs, the photons resulting from their annihilations within DM haloes should have energies in the gamma-ray range, hence detectable by instruments such as the *Fermi* Large Area Telescope (Atwood et al. 2009, LAT) or the ground based IACTs like HESS, VERITAS or MAGIC (Zitzer 2015, Ahnen et al. 2016, Giammaria et al. 2016, Morå 2015). Indeed, in recent years many groups have used the LAT data in direction of dSphs to search for γ-ray signals (Ackermann et al. 2011, Ackermann et al. 2015, Geringer-Sameth et al. 2015b, Drlica-Wagner et al. 2015).

In these analyses equation (1) is used to extract limits on $\langle\sigma v\rangle$ from the data for a range of $m_{\rm DM}$. The viable DM masses are usually suggested by standard model extensions (SMEs), which also give the spectrum of the possible annihilation channels i (for a recent review on the various SMEs see Rodrigues da Silva 2014). The remaining quantity to be determined is the J-factor; this term represents the major systematic uncertainty in DM searches. The now-standard technique for determining the J-factor involves a likelihood-based fitting to the stellar photometric and kinematic data within a Bayesian framework. The stellar and DM distributions are typically assumed to be spherically-symmetric, but possibly with anisotropic stellar velocity distribution. A Markov Chain Monte Carlo (MCMC) is used to sample the posterior probability distribution function of the J-factor for a given choice of the parameters assumed in $\rho_{\rm DM}$ (Martinez et al. 2009, Martinez 2015, Bonnivard et al. 2015, Geringer-Sameth et al. 2015a, Bonnivard et al. 2016, Ullio & Valli 2016). However, in cases of small stellar data samples, the determination of the J-factor is subject to the choice of theoretical priors (Martinez et al. 2009). This shortcoming is not present in a frequentist treatment of the problem.

From the perspective of kinematic modelling of the data, several authors have recently proposed improvements upon this standard spherically-symmetric analysis, and have explored the implications for current and future gamma-ray observations. Bonnivard et al. (2015) use mock kinematic data with underlying triaxial DM haloes, and analyse the data under the assumption of the spherically-symmetric Jeans equation. They identify biased J-factor estimates for the mildly triaxial halo models they consider. Hayashi et al. (2016) consider an axisymmetric Jeans model. Sanders et al. (2016) consider a flattened model for the stellar and DM distribution, and estimate the correction for the J-factor relative to spherical models for prolate and oblate DM haloes. Each of these models that utilize the axisymmetric Jeans equations requires model-dependent assumptions on the three-dimensional shape of the DM density distribution, and where necessary assume a Gaussian likelihood function for the stellar velocities.

In this paper we adhere with the assumption of spherical symmetry, but differ from the standard modelling by presenting the first fully frequentist derivation of the dSphs J-factor based on the profile likelihood technique. This approach has two main advantages: first, it avoids the additional systematic uncertainty introduced by the choice of priors in a Bayesian analysis and secondly, it allows a more consistent treatment of J-factor uncertainties in gamma-ray analyses which mostly are frequentist. We explicitly compare and contrast to the results from previous Bayesian analyses.

This paper is organized as follows. Section 2 describes our analysis method in detail. Section 3 presents a validation of this technique based on the simulations produced by the *Gaia* Challenge team. In Section 4 we calculate the J-factor for 20 dSphs, compare our results to previously obtained values available in the literature, and also discuss the properties of our results and the validation. We conclude with a discussion on future prospects for DM searches and possible improvements of the technique.

2 METHOD

For the l.o.s. stellar velocity data we assume a Gaussian likelihood function of the form (Walker et al. 2006, Strigari et al. 2008):

$$\mathcal{L} = -\log L = \frac{1}{2}\sum_{i=1}^{N_\star}\left[\frac{(v_i-u)^2}{\sigma_i^2} + \log(2\pi\sigma_i^2)\right] \quad , \qquad (3)$$

where the index i runs over each of the $N_\star$ stars in the sample, and where v_i and u are the particular and mean velocity, respectively. The expected velocity dispersion σ_i is taken as the squared sum of a measurement uncertainty ϵ_i and a l.o.s. systemic dispersion $\sigma_{\rm los}(R_i)$, which depends on the projected radial distance of star i to the centre of the system: $\sigma_i^2 = \epsilon_i^2 + \sigma_{\rm los}^2(R_i)$. We note that the Gaussian likelihood function in equation (3) is likely an approximation to the probability distribution for a true stellar velocity at a projected position, which is ultimately a function of the dynamical model for the stars and the DM. For dSphs in which the true velocity dispersion is similar to the dispersion from the measurement uncertainty, such as ultra-faint dwarfs, σ_i is dominated by Gaussian measurement uncertainty, so equation (3) is a good approximation.

The second assumption of our analysis, which is again standard, is the spherical Jeans equation (Binney & Tremaine 2008). This is used to link $\sigma_{\rm los}^2(R_i)$ to the underlying gravitational potential, assumed to be entirely defined by the DM halo density profile. The solution of the spherical Jeans equation for the l.o.s. velocity dispersion is

$$\sigma_{\rm los}^2(R) = \frac{2}{I(R)}\int_R^\infty\left(1-\beta(r)\frac{R^2}{r^2}\right)\frac{r}{\sqrt{r^2-R^2}}\frac{1}{f(r)} \times \int_r^\infty f(s)\frac{\nu_\star(s)\mathrm{GM}(s)}{s^2}\mathrm{d}s\,\mathrm{d}r \quad , \qquad (4)$$

with

$$f(r) = f_{r'}\exp\left[\int_{r'}^r \frac{2\,\beta(t)}{t}\mathrm{d}t\right] \quad . \qquad (5)$$

Here, R is the projected distance from the star to the centre of the stellar system; $M(s) = 4\pi\int_0^s \rho_{DM}(r)r^2\mathrm{d}r$ is the total enclosed DM mass; $\nu_\star$ is the density profile of the luminous component of the system, $I(R)$ its corresponding surface brightness, and $\beta(r)$ is the velocity anisotropy profile.

Inferring $\rho_{\rm DM}(r)$ from stellar data, usually in the form of a parametrized function, directly allows for the computation of the J-factor in equation (2). In the literature, this inference proceeds via a Bayesian analysis which samples (via MCMC for instance) a posterior probability density built

from equation (3) and a prior density that captures further information (Martinez et al. 2009, Geringer-Sameth et al. 2015a, Bonnivard et al. 2016). Marginalization of the parameters eventually yields the J-factor probability density by direct integration.

Alternatively, it is straightforward to derive a likelihood function dependent on the J-factor directly, and to draw inference from it. To do so, we note that the parametrized functions defining $\rho_{\rm DM}(r)$ are generically first order polynomials in a scale density parameter ρ_0, while also depending on a scale radius r_0, so that one can write $M(s, r_0, \rho_0) = \rho_0\, m(s, r_0)$ and $J(r_0, \rho_0, D, \Delta\Omega) = \rho_0^2\, j(r_0, D, \Delta\Omega)$. Then, simply replacing $M(s, r_0, \rho_0)$ in equation (4) by $\sqrt{J/j(r_0, D, \Delta\Omega)}\, m(s, r_0)$ yields the desired formalism for a direct likelihood analysis on the parameter J.

To completely determine the problem, one needs to adopt a specific functional expression for $\rho_{\rm DM}(r)$, $\nu_\star(r)$ and $\beta(r)$. Here we use the generalized Hernquist profile (Hernquist 1990):

$$\nu_\star(r) = \rho_\star \left(\frac{r}{r_\star}\right)^{-\gamma} \left(1 + \left(\frac{r}{r_\star}\right)^{\alpha}\right)^{-\frac{\beta-\gamma}{\alpha}} \quad , \qquad (6)$$

for both $\rho_{\rm DM}$ and $\nu_\star$ (with the '$\star$' subscript replaced by '0' for $\rho_{\rm DM}$), with the following prescription. The DM is either a cusped or cored Zhao profile (Zhao 1996), corresponding to $(\alpha, \beta, \gamma) = (1, 3, 1)$ or $(1, 3, 0)$; the former corresponds to the well-known NFW profile (Navarro et al. 1997). For the light profile $I(R)$, we make use of either a Plummer (Plummer 1911), Plummer-like, or non-Plummer profiles, which are obtained via the Abel transform[1] of equation (6) with $(\alpha, \beta, \gamma) = (2, 5, 0)$, $(2, 5, 0.1)$, or $(2, 5, 1)$, respectively. Observing equation (4), we notice that $\nu_\star / I(R)$ is independent of the normalization parameter $\rho_\star$, which can thus be arbitrarily set to unity.

Finally, we consider here three parameterizations for $\beta(r)$: an isotropic stellar velocity distribution with $\beta(r) = 0$, a constant anisotropy with $\beta(r) = \beta$, and an Osipkov-Merritt profile (OM, Osipkov 1979, Merritt 1985)

$$\beta(r) = \frac{r^2}{r^2 + r_a^2} \quad . \qquad (7)$$

In this formula r_a is the scale radius at which the velocity profile shifts from isotropic to anisotropic. The choice for the OM profile is further discussed below. We are interested in the maximum likelihood estimate (MLE) and likelihood curve for the J-factor, J, with the scale radius parameters, r_0, $r_\star$, and the value of β or r_a in the two last anisotropy scenarios playing the role of nuisance parameters.

With these ingredients in mind, we fit for J with a profile likelihood technique that also yields the likelihood curve. For each fixed value of J scanned over a reasonable range, we minimize the resulting likelihood function $\mathcal{L}_J(\vec{\rm R}, \vec{\rm v}, \vec{\epsilon}\,|\,\vec{g})$ with respect to the nuisance parameters $\vec{g}$, thus obtaining, by interpolation, the likelihood curve over J together with its minimum. For data (Sec. 4), $r_\star$ is always fixed to its value in the literature (McConnachie 2012), whereas for simulations (Sec. 3), to its true value. In the notation above, the nuisance parameter vector $\vec{g}$ always includes r_0, plus β or r_a depending on the anisotropic stellar velocity profile assumed. Fitting a different profile than simulated, or freeing structural parameters (e.g. the three exponents of the Zhao profile) is left for a future work. The vectors $(\vec{R}, \vec{v}, \vec{\epsilon})$ stand for the data arrays associated with each dSph (radius, velocity, and velocity measurement uncertainty, respectively; see McConnachie 2012, Walker 2013, Battaglia et al. 2013, Strigari 2013 for further reference on the dSphs stellar data). The minimization is performed with the MINUIT[2] library. Given the scale range of the J-factor that we need to consider, we actually fit the parameter $\mathcal{J} = \log_{10}({\rm J})$ instead of J. Fig. 1 shows the likelihood curve $\mathcal{L}(\mathcal{J})$ obtained with our procedure in the case of the Draco dSph, when assuming an isotropic stellar velocity distribution.

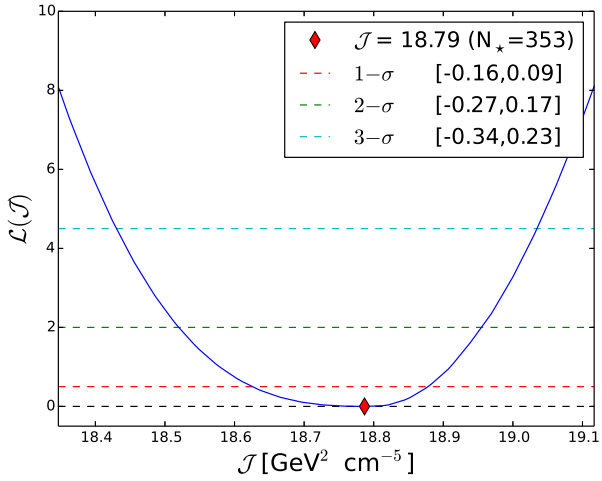

Figure 1. Profile likelihood of $\mathcal{J}$ obtained from the application of the MLE scheme on the stellar data of Draco (see text). An isotropic model for the stellar velocity distribution was assumed.

3 VALIDATION

In order to obtain $\mathcal{L}(\mathcal{J})$ by applying the MLE scheme outlined in the previous section, we have developed a PYTHON code called ASTROJPY [3]. We validate the procedure by running our code on the simulated data produced by the *Gaia* Challenge team [4] (Walker & Peñarrubia 2011). These simulations are designed to mimic spherical and triaxial collisionless stellar systems belonging to, e.g., the Milky Way, its dSphs, or giant elliptical galaxies. They were generated to provide a verification tool for the mass modelling of the systems that the *Gaia* satellite is currently observing (de Bruijne 2012). They consist of random samplings from a stellar distribution function model. Here we focus on spherically symmetric models, for the DM adopting cusped and

[1] The expression of the Abel transform for the projection of a quantity $f(r)$ into $F(R)$ reads $F(R) = 2\int_R^{+\infty} \frac{f(r) r dr}{\sqrt{r^2 - R^2}}$, where R is the projected radius.

[2] We used the iminuit python implementation: https://pypi.python.org/pypi/iminuit.

[3] ASTROJPY will be soon released to the public. The interested reader is welcome to contact the authors.

[4] http://astrowiki.ph.surrey.ac.uk/dokuwiki/doku.php?id=workshop

Table 1. Models tested with the MLE scheme. For each, our code was run on the 100 and 1000 star data sets. All models assume $r_0 = 1$ kpc.

Model	ρ_0 ($M_\odot kpc^{-3}$)	$\mathcal{J}$ (GeV^2 cm^{-5})	r_a (kpc)	γ	$r_\star$ (kpc)
OM Cored non-Plummer	4×10^8	19.23	0.25	1	0.25
OM Cored Plummer-like	4×10^8	19.23	0.25	0.1	0.25
Isotropic Cored non-Plummer	4×10^8	19.23	∞	1	1
Isotropic Cored Plummer-like	4×10^8	19.23	∞	0.1	1
OM Cusped non-Plummer	6.4×10^7	18.83	0.1	1	0.1
OM Cusped Plummer-like	6.4×10^7	18.83	0.1	0.1	0.1
Isotropic Cusped non-Plummer	6.4×10^7	18.83	∞	1	0.25
Isotropic Cusped Plummer-like	6.4×10^7	18.83	∞	0.1	0.25

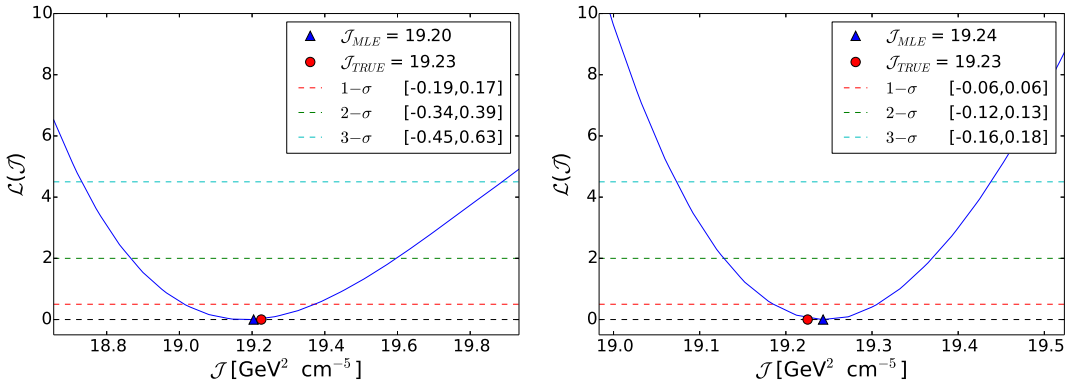

Figure 2. Results of the MLE scheme applied on the *Gaia* Challenge mock data sets of the Isotropic Cored Plummer-like model. The plot on the left (right) was obtained using the 100 (1000) stars sample. The likelihood curves were obtained assuming the true model in equation 4 and profiling over the nuisance parameter array $\vec{g}$ (see text).

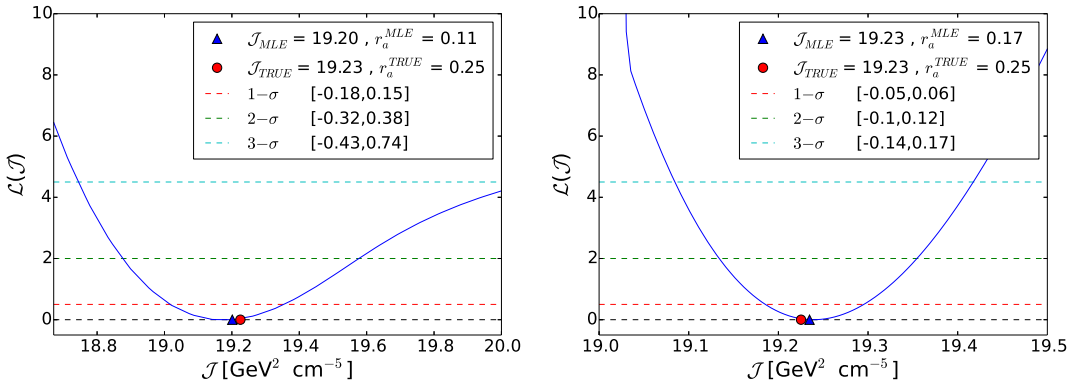

Figure 3. Results of the MLE scheme applied on the *Gaia* Challenge mock data sets of the OM Cored non-Plummer anisotropic model. The plot on the left (right) was obtained using the 100 (1000) stars sample. The likelihood curves were obtained assuming the true model in equation 4 and profiling over the nuisance parameter array $\vec{g}$ (see text).

cored Zhao profiles, and for the stars adopting the Plummer-like or non-Plummer profiles as is described above (Sec. 2).

The *Gaia* Challenge simulations were generated from a stellar distribution function assuming an OM anisotropy profile, so for our mock data we work within the context of this model. In order to generate an isotropic model from these simulations, we consider the fiducial model with $r_a = \infty$. Models with variable anisotropy are obtained by setting r_a to a value similar to the characteristic scale in the light distribution, $r_\star$.

As we would like the *Gaia* Challenge simulations to resemble the properties of observed dSphs as much as possible, mock systems would be ideally built with velocity dispersions of $\approx 5 - 10$ km s^{-1}, roughly constant at all projected radii from the centre of the dSphs. For example, models with substantial radial velocity anisotropies have observed velocity dispersions that vary much more than the corresponding profiles of the observed dSphs. Thus, in our choice of fiducial models, we must balance the fact that we are considering a specific OM anisotropy profile with the fact that we are constrained to mimic the actual dSph data.

Motivated by these considerations we choose a set of

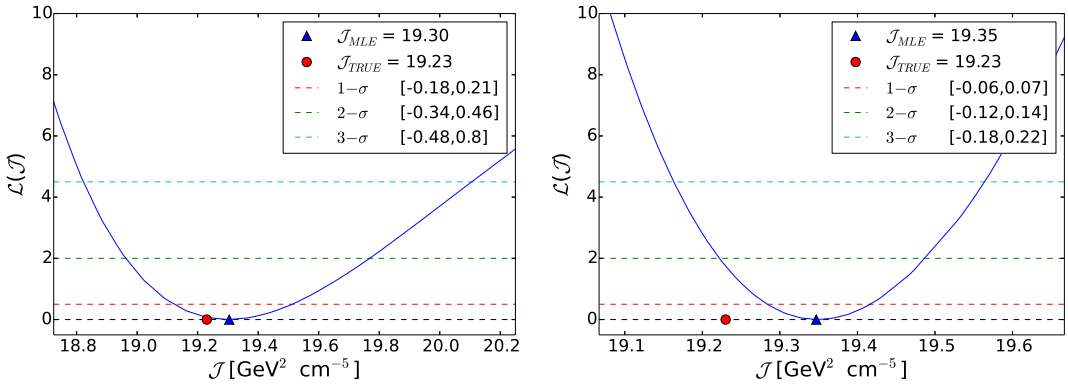

Figure 4. Results of the MLE scheme applied on the *Gaia* Challenge mock data sets of the Isotropic Cored Plummer-like model. The plot on the left (right) was obtained using the 100 (1000) stars sample. The likelihood curves were obtained assuming the Isotropic NFW Plummer model, thus the same model used on dSphs data, and profiling over the nuisance parameter array $\vec{g}$ (see text).

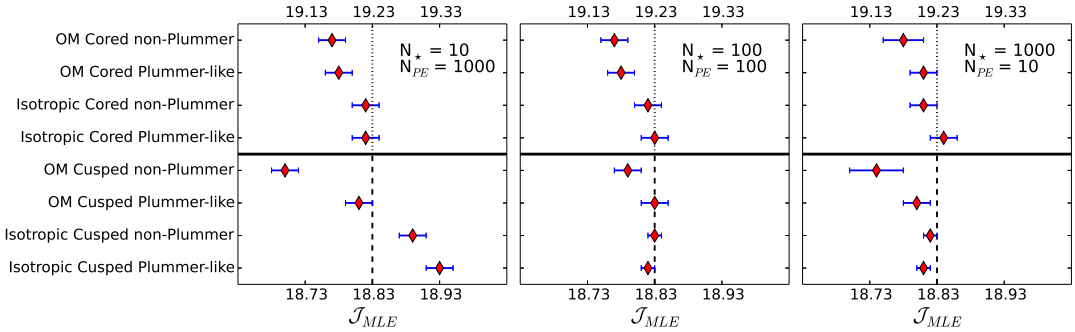

Figure 5. Bias estimates for the eight models provided by *Gaia* Challenge. The red dots represent the mean values of the $\mathcal{J}_{\rm MLE}$ obtained in the pseudo-experiments (PE) generated by partitioning the full data set (see text for details). The errorbars are the 1σ uncertainties on these means. The dashed (dotted) vertical lines indicate $\mathcal{J}_{\rm TRUE}$ of the cusped (cored) models (see Table 1).

eight different models, which are shown in Table 1. In our tests we use simulated data sets of 100 and 1000 stars generated from the appropriate distribution functions. We project the three-dimensional sets of positions and velocities generated from the distribution function along their z-axis, and set the distance to the centre of the simulated dSphs to a value of $D = 100$ kpc.

Assuming the true model in equation (4), we let the code retrieve the true $\mathcal{J}$ factor ($\mathcal{J}_{\rm TRUE}$), integrating up to $\theta_{\rm max} = 0.5^\circ$ in equation (2) and assuming the same distance D, while profiling over the nuisance parameters $\vec{g}$. The results of the tests for one isotropic model and one anisotropic model are shown in Figs. 2 and 3. In both figures, the plots on the left (right) column were obtained using the 100 (1000) stars data sets. We notice that the uncertainty in the best fitting values ($\mathcal{J}_{\rm MLE}$) consistently decreases with growing sample size, as evident from the narrowing of the confidence intervals. Moreover, $\mathcal{J}_{\rm MLE}$ approaches $\mathcal{J}_{\rm TRUE}$ as $N_\star$ grows, as seen by comparing the left plots with the right ones in Figs. 2 and 3. A similar trend occurs for the nuisance parameters, as shown, e.g., for the anisotropy parameter r_a in the legends of Fig. 3. The results for the other six models examined (not shown) exhibit a similar behaviour.

To assess the statistical robustness of our method at different $N_\star$, we partition the full mock data set (10^4 stars) three times, into subsets containing either 10, 100, or 1000 stars. Note that this yields many (1000) subsets for testing $N_\star = 10$, while only 10 sets are available for $N_\star = 1000$. With these, first we assessed the bias and evaluated its uncertainty. In Fig. 5 we show the mean value of the recovered $\mathcal{J}_{\rm MLE}$ for the eight models considered. In general the bias is smaller than 1 per cent. Notably, the bias is rather small even for $N_\star$ as low as 10, except for the case of an OM Cusped non-Plummer model. The somewhat larger bias for anisotropic models is likely due to the fact that while equation (3) is a good approximation to the isotropic case it does not correspond to the true likelihood implemented to generate the simulated data. Next, we tested the coverage of the confidence intervals for each of the eight models and three sample sizes, and summarize the results in Fig. 6. The green band represents the range of expected coverage estimates. Notably, the method seems to provide over-coverage (i.e. is conservative) for the case with only 10 stars. The coverage is overall satisfactory and the most critical cases of under-coverage occur when including the anisotropy parameter in the analysis of the set of ten samples with $N_\star = 1000$. Part of the undercoverage can be due to problems minimizing the large and degenerate parameter space that results from the inclusion of the anisotropy parameter (as for the methodological test the fitting for individual cases is not optimized) and the above mentioned aspects that the likelihood model we use is not entirely correct in the anisotropic

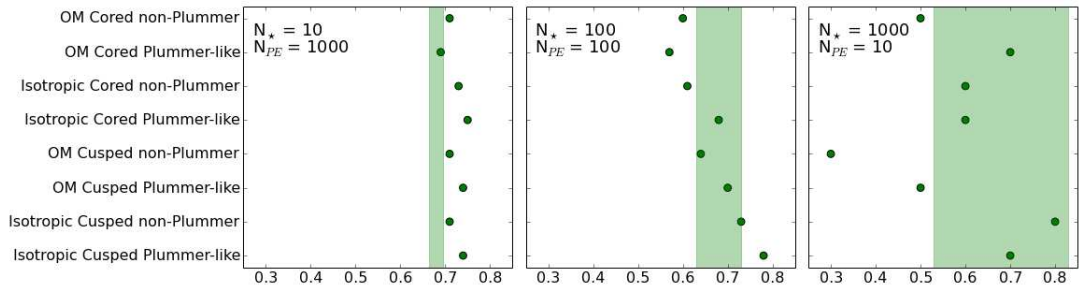

Figure 6. Results for the 1σ coverage test. The points represent the coverage of each of the eight models used in the validation (y-axis, see Table 1). The green bands represent the expected coverage of an ideal test, i.e. one which yields exactly 68 per cent.

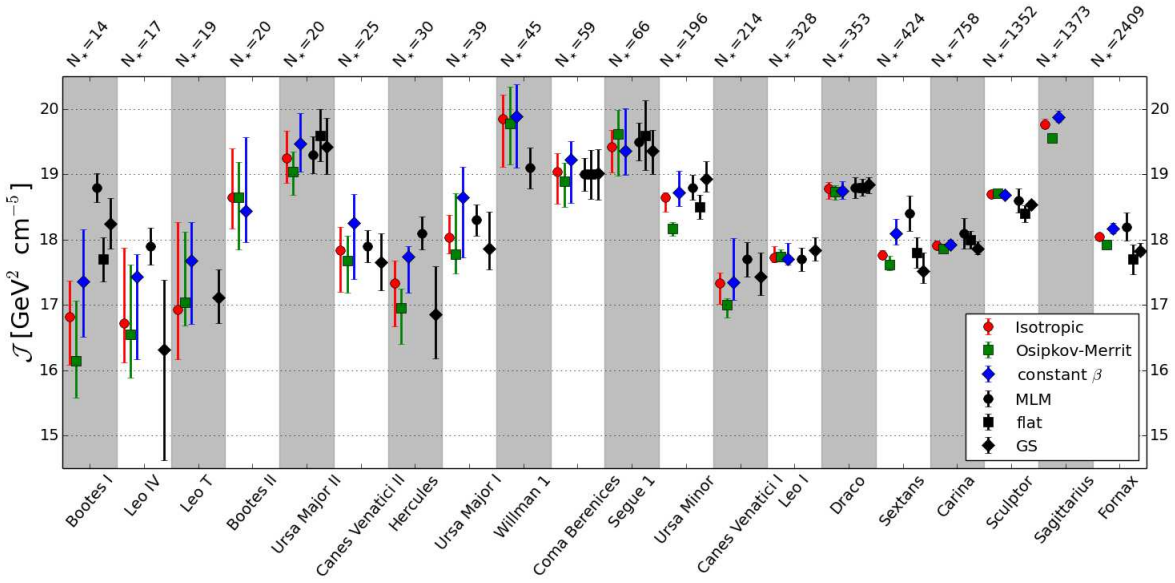

Figure 7. Results of the MLE scheme applied on the kinematic data from 20 dSphs using the three models for the stellar velocity anisotropy considered in this study: isotropic (red circles), constant β (blue diamonds) and Osipkov-Merrit (green squares). For all dSphs, the DM distribution and the stellar surface brightness in equation 4 corresponded to NFW and Plummer profiles. The black points refer to the results reported in Ackermann et al. (2011, flat) (squares), Ackermann et al. (2015, MLM) (cicles) and Geringer-Sameth et al. (2015a, GS) (diamonds) using Bayesian techniques (see text). The errorbars correspond to the 1-σ uncertainties.

case. In summary, despite the non-optimal modelling, the statistical properties are satisfactory and provide a strong indication of the reliability of the method and the statistical approach adopted.

The validation presented in this section was made assuming the true models used to create the mock data sets. Application of our method to real data incurs a new systematic uncertainty, because the true model is not known. The size of this uncertainty can be estimated by comparison with other methods, see, e.g. Fig. 7. More directly, we can repeat our analysis while assuming a different model than the one used to generate the mock data. We do so, calculating the $\mathcal{J}$ factor for the small and large (100 and 1000 stars) mock samples generated with the 'Isotropic Cored Plummer-Like' model, but assuming the 'Isotropic NFW Plummer' model, which we also use on real data (Sec. 4). The results of this exercise are shown in Fig. 4. We find the $\mathcal{J}$ factor to change by approximately 1 per cent, independent of the sample size. This uncertainty is not a characteristic of our frequentist method, and is rather a feature of the particular model space we are choosing. We expect this systematic to become smaller as more parameters of the DM profile are freed in the fit, and the model space becomes continuous.

4 RESULTS AND DISCUSSION

In this Section we present the results from the application of our scheme using kinematic data from 20 dSphs. In order to properly compare to previous Bayesian-based methods, we use the same kinematic data as in the previous *Fermi*-LAT analyses (Ackermann et al. 2011, 2015). In both of these

Table 2. $\mathcal{J}$ factors derived from the kinematic data of 20 dSphs assuming an isotropic (Iso), a constant anisotropy (Ca) and the Osipkov–Merrit (OM) stellar velocity anisotropy profiles, respectively. The uncertainties correspond to the 1σ errors obtained from the likelihood curve constructed with MLE scheme we have developed (see Sec. 2). The values in the second column indicate the number of stars in each data set.

Dwarf	$N_\star$	$\mathcal{J}_{\rm MLE}$(Iso)	$\mathcal{J}_{\rm MLE}$(Ca)	$\mathcal{J}_{\rm MLE}$(OM)
Bootes I	14	$16.82^{+0.55}_{-0.74}$	$17.36^{+0.79}_{-0.85}$	$16.15^{+0.92}_{-0.56}$
Leo IV	17	$16.73^{+1.15}_{-0.60}$	$17.44^{+0.34}_{-1.27}$	$16.55^{+1.07}_{-0.66}$
Leo T	19	$16.93^{+1.34}_{-0.76}$	$17.68^{+0.59}_{-0.97}$	$17.04^{+1.08}_{-0.35}$
Ursa Major II	20	$19.26^{+0.41}_{-0.38}$	$19.47^{+0.46}_{-0.43}$	$19.05^{+0.30}_{-0.36}$
Bootes II	20	$18.64^{+0.75}_{-0.47}$	$18.44^{+1.13}_{-0.48}$	$18.65^{+0.54}_{-0.80}$
Canes Venatici II	25	$17.83^{+0.36}_{-0.63}$	$18.25^{+0.44}_{-0.86}$	$17.68^{+0.38}_{-0.49}$
Hercules	30	$17.33^{+0.35}_{-0.66}$	$17.74^{+0.16}_{-0.55}$	$16.96^{+0.29}_{-0.55}$
Ursa Major I	39	$18.03^{+0.34}_{-0.24}$	$18.65^{+0.46}_{-0.92}$	$17.78^{+0.93}_{-0.30}$
Willman 1	45	$19.86^{+0.36}_{-0.74}$	$19.89^{+0.48}_{-0.79}$	$19.77^{+0.57}_{-0.62}$
Coma Berenices	59	$19.05^{+0.28}_{-0.49}$	$19.22^{+0.28}_{-0.66}$	$18.90^{+0.28}_{-0.40}$
Segue 1	66	$19.42^{+0.26}_{-0.39}$	$19.36^{+0.66}_{-0.36}$	$19.62^{+0.37}_{-0.64}$
Ursa Minor	196	$18.64^{+0.08}_{-0.22}$	$18.73^{+0.33}_{-0.21}$	$18.17^{+0.10}_{-0.11}$
Canes Venatici I	214	$17.33^{+0.16}_{-0.32}$	$17.35^{+0.68}_{-0.27}$	$17.01^{+0.10}_{-0.20}$
Leo I	328	$17.73^{+0.17}_{-0.08}$	$17.70^{+0.25}_{-0.08}$	$17.74^{+0.11}_{-0.07}$
Draco	353	$18.79^{+0.09}_{-0.16}$	$18.75^{+0.15}_{-0.13}$	$18.73^{+0.10}_{-0.12}$
Sextans	424	$17.76^{+0.08}_{-0.06}$	$18.10^{+0.21}_{-0.18}$	$17.61^{+0.14}_{-0.08}$
Carina	758	$17.91^{+0.08}_{-0.05}$	$17.95^{+0.04}_{-0.08}$	$17.86^{+0.07}_{-0.05}$
Sculptor	1352	$18.70^{+0.03}_{-0.04}$	$18.68^{+0.04}_{-0.03}$	$18.71^{+0.05}_{-0.06}$
Sagittarius	1373	$19.77^{+0.08}_{-0.07}$	$19.88^{+0.10}_{-0.08}$	$19.56^{+0.06}_{-0.07}$
Fornax	2409	$18.04^{+0.03}_{-0.04}$	$18.17^{+0.08}_{-0.08}$	$17.93^{+0.05}_{-0.03}$

studies, the $\mathcal{J}$ factors and their uncertainties were obtained by sampling the posterior likelihood, using flat priors on the DM density profile parameters, in the former, and multi-level modelling (MLM) by Martinez (2015) in the latter.

Our analysis assumes an NFW profile for the DM density, a Plummer profile for the surface brightness of the dSphs and one of the three velocity anisotropy profiles defined in Sec. 2. Similar to the assumptions in the *Fermi*-LAT analyses, we fix the angular integration angle to $\theta_{\rm max} = 0.5^\circ$. For most of the brightest dSphs, this roughly corresponds to the half-light radius of the projected stellar distribution. It is within this approximate angular region that the integrated DM mass, and the J-factor, are most strongly constrained from the Jeans equations (Wolf et al. 2010, Walker et al. 2011). Furthermore, this is the region where most of the annihilation signal is expected to originate (Strigari et al. 2007, Sanchez-Conde et al. 2011).

The MLE of $\mathcal{J}$ together with their 1-σ uncertainties are presented in Table 2. In Fig. 7, (where possible) we compare our results for all three velocity anisotropy models assumed (colored points) with previous results (black points) from Ackermann et al. (2011, 2015), as well as from Geringer-Sameth et al. (2015a). The later results from Geringer-Sameth et al. (2015a) are similar to the flat prior case considered in Ackermann et al. (2011), though the former marginalizes over a larger set of parameters that describe the DM profile.

We note that the uncertainties on the Bayesian results (i.e. the error bars of the black points) are reflective of both the statistical uncertainties and the assumed priors. This becomes evident when noting that the errors are weakly dependent on the size of the sample of stars. By contrast, for our method the confidence intervals decrease with the sample size, as expected from statistical uncertainties. For most dSphs, there is broadly good agreement with the previous Bayesian-derived results. The biggest deviations occur for Bootes 1, in particular in comparison to the MLM analysis. We believe that this is mostly due to the assumed prior in the MLM analysis.

The overall spread in the best-fitting values for the $\mathcal{J}$ factors obtained from different methods illustrates the systematic impact of our modelling. The $\mathcal{J}$ factor is relatively insensitive to our model assumptions, with a maximum difference of 7 per cent for Bootes I. The overall spread between the different estimates can be taken as a rough indication of overall systematic uncertainties. In this particular comparison, it can be seen that the spread is roughly comparable to the statistical uncertainties for dwarfs with less than about 100 stars, whereas the systematic uncertainties dominate for the brightest dwarfs.

We reiterate that our results have been obtained assuming a particular model for the DM density, stellar and velocity anistropy profiles. This resulted in the reduction of the dimensionality of the full parameter space of the problem, hence in the size of the parameters array fit by MINUIT. Relaxing some of these assumptions and fitting a broader parameter space would allow the investigation of possible deviations from the model used, at the expense of reintroducing the degeneracy between the various profiles parameters. The effect of this modification and of the systematic effects arising from different model assumptions will be studied in a future project. Finally, though the likelihood function that we utilize does not lend itself to a straightforward definition of goodness-of-fit, we have checked that for all dSphs we study the best-fitting velocity dispersion profiles provide an acceptable χ^2 per degree of freedom in comparison to the binned velocity dispersion data.

5 CONCLUSIONS

In this paper, we show that J-factor estimates and proper confidence intervals can be derived from stellar data with a completely frequentist Jeans analysis, based on a profile likelihood methodology. We validate this procedure with mock data sets from the *Gaia* Challenge, and present prior-free estimates of the J-factors for 20 dSphs, removing the systematic uncertainty introduced by the often arbitrary choice of priors. Note that we do not attempt to compare the precision of our estimates with those in literature as this is only meaningful under similar model assumptions. We simply conclude that our method provides the desired statistical properties. In principle, there is no limitation to the extension of our method to more general models, depending on the envisaged application. Furthermore, this method opens the way to a correct definition of the likelihood function, essential for a self-consistent treatment of DM searches with gamma-ray data, which are predominantly performed in a frequentist framework. In future work we will update such gamma-ray analyses, provide a detailed study of the aforementioned systematic uncertainties compared to prior-

based derivation, and extend the framework to non-Gaussian assumptions on velocity sampling distributions. Additional improvement may be obtained by appealing the measured distribution of Milky Way foreground stars (Ichikawa et al. 2016), which can be particularly important for dSphs with small kinematic samples.

ACKNOWLEDGEMENTS

AC is thankful to H. Silverwood and to M. Meyer for useful discussions. JC-T acknowledges the support of the Laboratoire de Physique Corpusculaire de Clermont-Ferrand, where part of this work was done. JC thanks support from the Knut and Alice Wallenberg foundation, Swedish Research Council and Swedish National Space Board. LES acknowledges support from NSF grant PHY-1522717. BA acknowledges the support from the Swedish Research Council (PI: J. Conrad). MASC is a Wenner-Gren Fellow and acknowledges the support of the Wenner-Gren Foundations to develop his research.

REFERENCES

Ackermann M., et al., 2011, Phys. Rev. Lett., 107, 241302
Ackermann M., et al., 2015, Phys. Rev. Lett., 115, 231301
Ahnen M. L., et al., 2016, JCAP, 1602, 039
Ajello M., et al., 2016, Astrophys. J., 819, 44
Atwood W. B., et al., 2009, ApJ, 697, 1071
Battaglia G., Helmi A., Breddels M., 2013, New Astron. Rev., 57, 52
Bertone G., Hooper D., Silk J., 2005, Phys. Rept., 405, 279
Binney J., Tremaine S., 2008, Galactic Dynamics: Second Edition. Princeton University Press
Bonnivard V., Combet C., Maurin D., Walker M. G., 2015, MNRAS, 446, 3002
Bonnivard V., Hütten M., Nezri E., Charbonnier A., Combet C., Maurin D., 2016, Comput. Phys. Commun., 200, 336
Calore F., Cholis I., Weniger C., 2015, JCAP, 1503, 038
Charles E., et al., 2016, Phys. Rept., 636, 1
Conrad J., 2014, in Interplay between Particle and Astroparticle physics London, United Kingdom, August 18-22, 2014. (arXiv:1411.1925), http://inspirehep.net/record/1326617/files/arXiv:1411.1925.pdf
Conrad J., Cohen-Tanugi J., Strigari L. E., 2015, J. Exp. Theor. Phys., 121, 1104
Drlica-Wagner A., et al., 2015, Astrophys. J., 809, L4
Feng J. L., 2010, Ann. Rev. Astron. Astrophys., 48, 495
Geringer-Sameth A., Koushiappas S. M., Walker M., 2015a, Astrophys. J., 801, 74
Geringer-Sameth A., Koushiappas S. M., Walker M. G., 2015b, Phys. Rev., D91, 083535
Giammaria P., Aleksić J., Lombardi S., Maggio C., Palacio J., Rico J., Vanzo G., Vazquez Acosta M., 2016, J. Phys. Conf. Ser., 718, 042024
Hayashi K., Ichikawa K., Matsumoto S., Ibe M., Ishigaki M. N., Sugai H., 2016, Mon. Not. Roy. Astron. Soc., 461, 2914
Hernquist L., 1990, Astrophys. J., 356, 359
Ichikawa K., Ishigaki M. N., Matsumoto S., Ibe M., Sugai H., Hayashi K., 2016, Foreground effect on the J-factor estimation of classical dwarf spheroidal galaxies (arXiv:1608.01749)
Martinez G. D., 2015, MNRAS, 451, 2524
Martinez G. D., Bullock J. S., Kaplinghat M., Strigari L. E., Trotta R., 2009, JCAP, 0906, 014
McConnachie A. W., 2012, AJ, 144, 4
Merritt D., 1985, AJ, 90, 1027
Morå K., 2015, in 27th Rencontres de Blois on Particle Physics and Cosmology Blois, France, May 31-June 5, 2015. (arXiv:1512.00698), https://inspirehep.net/record/1407811/files/arXiv:1512.00698.pdf
Navarro J. F., Frenk C. S., White S. D. M., 1997, Astrophys. J., 490, 493
Osipkov L. P., 1979, Soviet Astronomy Letters, 5, 42
Plummer H. C., 1911, MNRAS, 71, 460
Rodrigues da Silva P. S., 2014, A Brief Review on WIMPs in 331 Electroweak Gauge Models (arXiv:1412.8633)
Sanchez-Conde M. A., Cannoni M., Zandanel F., Gomez M. E., Prada F., 2011, JCAP, 1112, 011
Sanders J. L., Evans N. W., Geringer-Sameth A., Dehnen W., 2016, Phys. Rev., D94, 063521
Strigari L. E., 2013, Phys. Rept., 531, 1
Strigari L. E., Koushiappas S. M., Bullock J. S., Kaplinghat M., 2007, Phys. Rev., D75, 083526
Strigari L. E., Bullock J. S., Kaplinghat M., Simon J. D., Geha M., Willman B., Walker M. G., 2008, Nature, 454, 1096
Ullio P., Valli M., 2016, JCAP, 1607, 025
Walker M., 2013, Dark Matter in the Galactic Dwarf Spheroidal Satellites. p. 1039, doi:10.1007/978-94-007-5612-0_20
Walker M. G., Peñarrubia J., 2011, ApJ, 742, 20
Walker M. G., Mateo M., Olszewski E. W., Bernstein R. A., Wang X., Woodroofe M., 2006, Astron. J., 131, 2114
Walker M. G., Combet C., Hinton J. A., Maurin D., Wilkinson M. I., 2011, Astrophys. J., 733, L46
Wolf J., Martinez G. D., Bullock J. S., Kaplinghat M., Geha M., Munoz R. R., Simon J. D., Avedo F. F., 2010, Mon. Not. Roy. Astron. Soc., 406, 1220
Zhao H., 1996, Mon. Not. Roy. Astron. Soc., 278, 488
Zhou B., Liang Y.-F., Huang X., Li X., Fan Y.-Z., Feng L., Chang J., 2015, Phys. Rev., D91, 123010
Zitzer B., 2015, in Fifth International Fermi Symposium Nagoya, Japan, October 20-24, 2014. (arXiv:1503.00743), https://inspirehep.net/record/1347106/files/arXiv:1503.00743.pdf
de Bruijne J. H. J., 2012, Ap&SS, 341, 31

This paper has been typeset from a TEX/LATEX file prepared by the author.